Available online at www.sciencedirect.com
SCIENCE DIRECT®
Journal of Power Sources 146 (2005) 287–293
JOURNAL OF POWER SOURCES
www.elsevier.com/locate/jpowsour

The effects of preparation condition and dopant on the electrochemical property for Fe-substituted Li_2MnO_3

Mitsuharu Tabuchi [a,*], Akiko Nakashima [a], Kazuaki Ado [a], Hikari Sakaebe [a], Hironori Kobayashi [a], Hiroyuki Kageyama [a], Kuniaki Tatsumi [a], Yo Kobayashi [b], Shiro Seki [b], Atsushi Yamanaka [b]

[a] *National Institute of Advanced Industrial Science and Technology (AIST), 1-8-31 Midorigaoka, Ikeda, Osaka 563-8577, Japan*
[b] *Central Research Institute of Electric Power Industry, 2-11-1 Iwadokita, Komae, Tokyo 201-8511, Japan*

Available online 28 April 2005

Abstract

The specific capacity of Fe-substituted Li_2MnO_3 ($Li_{1.2}Fe_{0.4}Mn_{0.4}O_2$) was improved by adjusting the preparation temperature of Fe–Mn co-precipitate below RT in order to suppress the spinel ferrite formation, which hinders the formation of homogeneous and reactive precursor. The degradation of discharge capacity with cycle could be suppressed by nominal 5% Al, Ni and Co doping. This means that Fe-substituted Li_2MnO_3 will be considered to be one of the near future positive electrodes for practical use by careful optimization of its preparation condition and chemical composition.

Keywords: Dopant; Fe-substituted Li_2MnO_3; Electrochemical property

1. Introduction

The positive electrode materials including iron ion have been studied energetically in order to avoid depletion of cobalt resources in $LiCoO_2$ with the development of large-scale lithium-ion battery. Although lithium iron phosphate ($LiFePO_4$) is one of the best candidates as a 3 V positive electrode for the above application, there are several valuable challenges for finding 4 V positive electrode material based on iron oxides. Among them, the following results are obtained: the degradation of electrochemical performance in $LiFe_xM_{1-x}O_2$ ($0 < x < 0.3$, M = Co [1] and Ni [2]) solid solutions, and some degree of Fe^{3+}/Fe^{4+} redox reaction with Co or Ni ion on charging at 4 V [3,4]. Delmas et al. proposed the Fe^{4+} ion stabilization model; the Fe^{4+} ion could be generated if it was surrounded with only Ni^{4+} ions [4]. However, there was no evidence whether the Fe^{3+}/Fe^{4+} redox voltage existed or not at 4 V without the oxidation/reduction of other 3d elements in the layered rock-salt structure. Hence, Fe-substituted Li_2MnO_3 ($LiFeO_2$–Li_2MnO_3 solid solution: $Li_{(4-y)/3}Mn_{(2-2y)/3}Fe_yO_2$, $0 < y < 1$) has been designed for extracting the Fe^{3+}/Fe^{4+} redox voltage [5,6], because Li_2MnO_3 has been well known as an electrochemically-inactive phase. In our previous report, Fe-substituted Li_2MnO_3 has been found to belong to a 4 V positive electrode material due to the appearance of the Fe^{3+}/Fe^{4+} redox voltage around 4 V [5,6]. Unfortunately, the specific capacity for $Li_{1.2}Fe_{0.4}Mn_{0.4}O_2$ was too small (70–80 mAh g^{-1} at low current density 7.5 mA g^{-1}) for practical use. In this work, careful optimization of preparation condition has been carried out, and some improvement of its electrochemical property at a typical current density (42 mA g^{-1}) is proposed. Some elements (Al, Ni, and Co) have been utilized as a dopant, the amount of which was about 5%, for examining their effect on the electrochemical data as shown previously in $LiNi_{0.475}Mn_{0.475}M_{0.05}O_2$ (M = Al, Ti, Co) [7].

* Corresponding author. Tel.: +81 72 751 9618; fax: +81 72 751 9714.
E-mail address: m-tabuchi@aist.go.jp (M. Tabuchi).

0378-7753/$ – see front matter © 2005 Elsevier B.V. All rights reserved.
doi:10.1016/j.jpowsour.2005.03.032

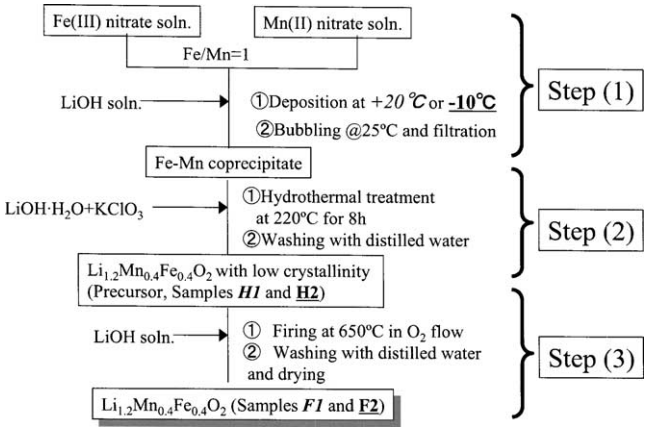

Fig. 1. Synthetic route for Fe-substituted Li_2MnO_3 ($Li_{1.2}Fe_{0.4}Mn_{0.4}O_2$). Samples F1 and F2 were obtained from samples H1 and H2, which were prepared from Fe–Mn co-precipitate deposited at +20 and −10 °C, respectively.

2. Experimental

Three steps were required for obtaining homogeneous $Li_{1.2}Fe_{0.4}Mn_{0.4}O_2$ samples (0.25 mol), as shown in Fig. 1.

(1) Fe–Mn co-precipitates were prepared by slowly dropping LiOH solution (50 g of $LiOH{\cdot}H_2O$ (>98% in purity) dissolved into 500 ml of distilled water) into mixed Fe–Mn nitrate solution (0.125 mol of $Fe(NO_3)_3{\cdot}9H_2O$ (>99.9% in purity) and $MnCl_2{\cdot}4H_2O$ (>99% in purity) dissolved into 500 ml of distilled water and 200 ml of ethanol) at +20 or −10 °C. Ethanol was added to avoid freezing the solution under cooling at −10 °C. The obtained co-precipitates were subjected to aging under air bubbling for 2 days at room temperature. The Fe–Mn co-precipitates were separated by filtration process.
(2) Low-crystallinity $Li_{1.2}Fe_{0.4}Mn_{0.4}O_2$ fine powder (precursors named samples H1 and H2) was formed by hydrothermal treatment of the above co-precipitates with an excess amount of $LiOH{\cdot}H_2O$ (50 g) and $KClO_3$ (50 g, >99.5% in purity) at 220 °C for 8 h. The precursors were purified by washing with distilled water, and then filtration and drying at 100 °C.
(3) The final products were obtained by firing the mixture of the precursor and an additional $LiOH{\cdot}H_2O$ (0.25 mol) in temperature ranging from 650 °C under oxygen flow. By washing with distilled water, filtration and then drying at 100 °C, each product was separated from residual salts.

$Co(NO_3)_2{\cdot}6H_2O$ or $Ni(NO_3)_2{\cdot}6H_2O$ added nominally 5 mol% (Ni/(Fe + Mn + Ni) and Co/(Fe + Mn + Co) = 0.05) into Fe–Mn nitrate solution in step (1) for homogeneous cation doping. Addition of 5 mol% Al source ($Al(NO_3)_3{\cdot}9H_2O$, Al/(Fe + Mn + Al) = 0.05) has been performed before firing in step 3, because Al^{3+} ion was dissolved into the solution under high pH condition.

The sample composition was estimated by Li, Fe, Mn, Al, Co, Ni elemental analysis using ICP spectrometer. Purity and cation distribution was checked by X-ray diffraction (XRD) measurement (Rigaku Rotaflex RU-200B/RINT) using monochromatized Cu Kα radiation within the 2θ range from 10 to 125°. The diffraction angle was calibrated using Silicon powder (SRM 640c) as an external standard. The program RIETAN-2000 [8] was used for structural refinement with X-ray Rietveld analysis. A split pseudo-Voigt profile function was selected for the pattern fitting. TEM observation (Hitachi, H-300) and BET specific surface area measurement (Quantachrome, Monosorb) characterized

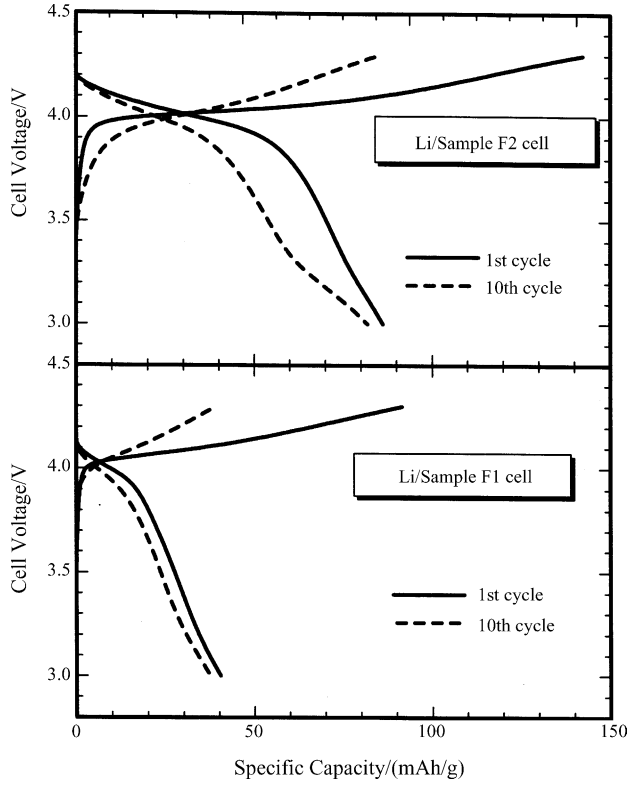

Fig. 2. First and tenth charge and discharge behaviour for two Li/sample cells between 3 and 4.3 V.

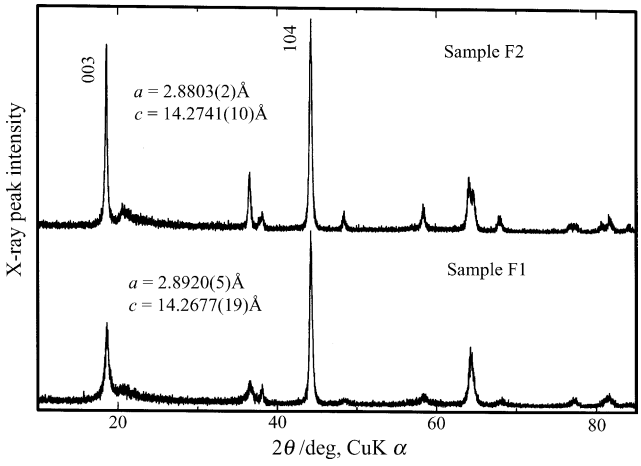

Fig. 3. XRD patterns of samples F1 and F2.

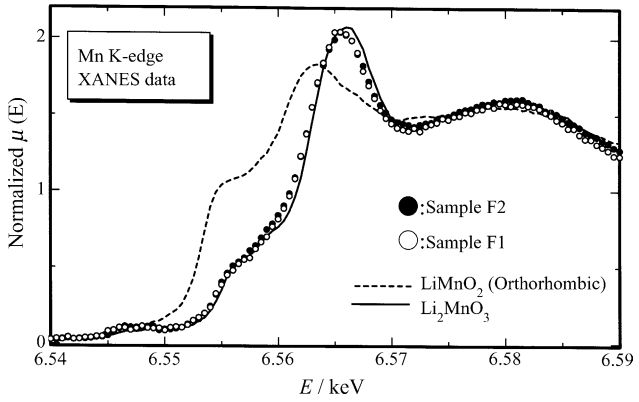

Fig. 4. Mn K-edge XANES spectra for samples F1 and F2 with two standard materials, $LiMnO_2$ and Li_2MnO_3. These materials are used for checking which Mn valency is 4+ or 3+.

the particle shape and average particle size, respectively. Magnetic field dependence of magnetization was measured at 300 K by Vibrating Sample Magnetometer (VSM, Riken Denshi) for determination of trace amount of magnetic impurity like spinel ferrite. $(NH_4)_2Mn(SO_4)_2{\cdot}6H_2O$ was used as a standard material for calibrating the magnetization. ^{57}Fe Mössbauer spectra were measured at 300 K. α-Fe foil calibrates the velocity axis. Each spectrum was fitted using symmetric doublets with Lorentzian line shape. Mn K-edge X-ray absorption near edge structure (XANES) spectra was measured by laboratory-type X-ray spectrometer (Technos, EXAC-820) in transmission mode at 293 K. Hydrothermally obtained $LiMnO_2$ (orthorhombic phase) and Li_2MnO_3 were used as reference materials.

Charge and discharge tests have been done using a positive electrode, which consisted of the sample (20 mg), acetylene black (5 mg) and PTFE powder (0.5 mg) between 3.0 and 4.3 V against the Li metal negative electrode at a fixed current density (42 mA g^{-1}), which corresponds to 1/3C rate for the ideal capacity (126 mAh g^{-1}). The complex impedance characterization of the cell was performed at 298 K using a multichannel potentiostat, Princeton Applied Research VMP2/Z. The applied AC signal for the electrochemical impedance spectroscopy (EIS) measurement was 10 mV, at a frequency between 200 and 50 mHz.

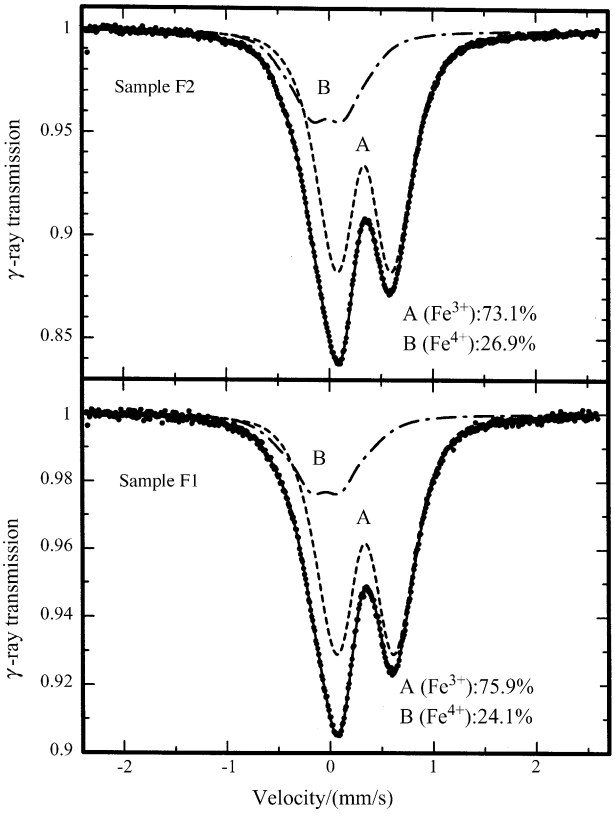

Fig. 5. Observed (●) and calculated (solid line) ^{57}Fe Mossbauer spectra for samples F1 and F2 at 300 K. Two symmetric doublets (broken and chain lines) named A and B used for constructing each calculated spectra. The former and latter components were assigned as Fe^{3+} and Fe^{4+} ones by there IS values, respectively.

3. Results and discussion

3.1. Effect of deposition temperature of Fe–Mn co-precipitate on electrochemical properties

In order to examine the effect of preparation temperature of Fe–Mn co-precipitate in step 1 on the electrochemical properties, two final products were selected. Samples F1 and F2 were obtained from the Fe–Mn co-precipitates, which was precipitated at +20 and −10 °C as shown in Fig. 1,

Table 1
^{57}Fe Mössbauer parameter at 300 K for samples F1 and F2 with standard materials with rock-salt related structure

Sample	Crystal structure	Component (area ratio)	IS (mm s^{-1})	QS[a] (mm s^{-1})
Sample F1	Layered rock-salt ($R\bar{3}m$)	A (Fe^{3+}, 75.9%)	+0.3413 (6)	0.573 (11)
		B (Fe^{4+}, 24.1%)	−0.039 (5)	0.33 (2)
Sample F2	Layered rock-salt ($R\bar{3}m$)	A (Fe^{3+}, 73.1%)	+0.3378 (4)	0.548 (11)
		B (Fe^{4+}, 26.9%)	−0.020 (4)	0.34 (2)
Layer-$LiFeO_2$ [9]	Layered rock-salt ($R\bar{3}m$)	–	+0.35	0.34
$LiCo_{0.8}Fe_{0.2}O_2$ [10]	Layered rock-salt ($R\bar{3}m$)	–	+0.32	0.31
α-$LiFeO_2$ [11]	Cubic rock-salt ($Fm\bar{3}m$)	–	+0.36	0.60
$Li_{1.2}Fe_{0.4}Ti_{0.4}O_2$ [11]	Cubic rock-salt ($Fm\bar{3}m$)	–	+0.36	0.62

[a] Each spectrum of both of samples F1 and F2 was fitted by two QS distributed doublets. The QS distribution analysis has been performed between 0 and 1.8 mm s^{-1} with a fixed line width of 0.2 mm s^{-1} for "A" component and between 0 and 1.5 mm s^{-1} with a fixed line width of 0.3 mm s^{-1} for "B" component.

respectively. For both the two, the hydrothermal and firing conditions were fixed to 220 °C for 8 h and 650 °C for 20 h. Only a crystalline phase with α-$NaFeO_2$ type structure ($R\bar{3}m$) was found in their XRD pattern. The chemical formula estimated by Li, Mn and Fe contents were $Li_{1.20}Fe_{0.41}Mn_{0.39}O_2$ for sample F1 and $Li_{1.22}Fe_{0.39}Mn_{0.39}O_2$ for Sample F2, indicating negligible discrepancy between them. However, a large difference in initial and 10th discharge capacities was observed between these two samples (Fig. 2). The initial and 10th discharge capacities for Li/sample F2 cell were twice as large as those for the other one.

To clarify the difference between them, the 3d metal ion distribution was estimated by X-ray Rietveld analysis, because large difference in 003/104 XRD peak ratios was observed in Fig. 3. A structural model: $(Li_{1-m}(Fe, Mn)_m)_{3a}[(Fe, Mn)_nLi_{1-n}]_{3b}O_2$ $(0<m<1, 0<n<1)$ was selected for the pattern fitting, in which Fe and Mn ions can exist on both Li (3a) and 3d metal (3b) sites. Cation distributions were estimated as $(Li_{0.863}M_{0.137(2)})_{3a}[M_{0.597(3)}Li_{0.403}]_{3b}O_2$ for sample F1 and $(Li_{0.9390}M_{0.0610(14)})_{3a}[M_{0.651(3)}Li_{0.349}]_{3b}O_2$ (M = Fe and/or Mn) for sample F2, and it indicated that the cation ordering degree in sample F2 is large compared with that in sample F1. Smaller amount of 3d cation (mostly Fe^{3+} ion [6]) in Li layer, which can prohibit fast Li^+ diffusion, may lead to the improvement of its specific capacity.

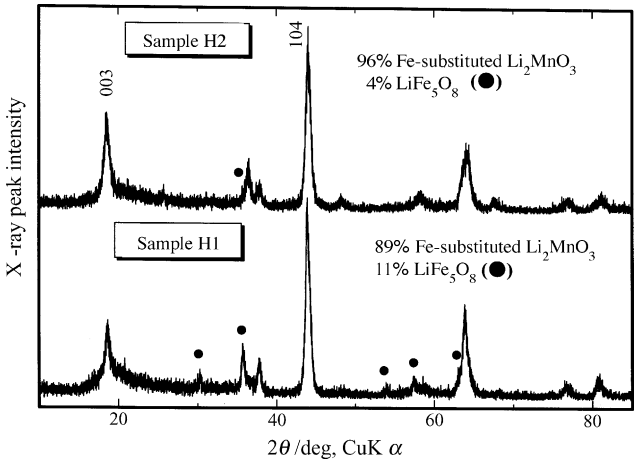

Fig. 6. XRD patterns for hydrothermally obtained samples H1 and H2. XRD peaks marked by closed circles were assigned as those of spinel ferrite with inverse spinel structure ($Fd\bar{3}m$). The other peaks correspond to Fe-substituted Li_2MnO_3 with layered rock-salt structure ($R\bar{3}m$).

By the way, it was found that Mn K-edge X-ray absorption spectra of both the samples were almost equivalent to that of the pristine one (Li_2MnO_3, Fig. 4), which means the tetravalent nature of Mn ions in both the samples. By numerical fitting ^{57}Fe Mössbauer spectra with two symmetric doublets (Fig. 5 and Table 1), the isomer shift (IS) values are

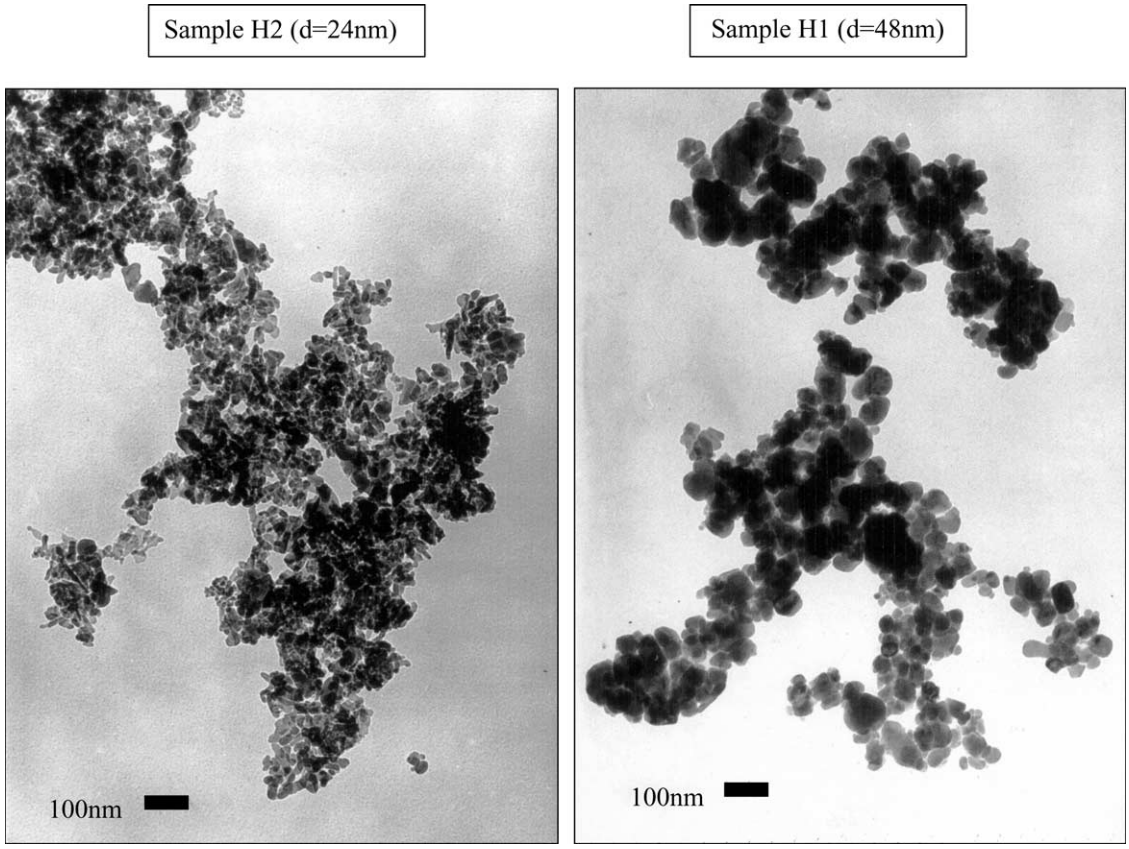

Fig. 7. TEM photographs for hydrothermally obtained samples H1 and H2: "d" means a symbol of average particle size estimated by their specific surface area.

+0.34 and −0.02 or −0.04 mm s^{-1} for components A and B, respectively. The former and latter IS values were close to those of Fe^{3+} (+0.33 mm s^{-1}) and Fe^{4+} (−0.11 mm s^{-1}) components in $Li_{0.28}Ni_{0.9}Fe_{0.1}O_2$ [4]. The area fraction of Fe^{4+} component (26.9%) for sample F2 was not so different from that for sample F1 (24.1%, see Fig. 5). Therefore, these spectral results imply that the difference in electrochemical behaviour could not be attributed with the difference in valence state of Mn and Fe ions.

The comparison of quadrupole splitting (QS) values between A and B components gave valuable information (Table 1); the QS value of B (Fe^{4+}) is very close to that of Fe ion existed in the transition metal layer (3b site) of layered rock-salt phase (layer-$LiFeO_2$[9], $LiCo_{0.8}Fe_{0.2}O_2$ [10]), whereas the QS value of A (Fe^{3+}) is close to that of the Fe ion existed in cubic rock-salt phase (α-$LiFeO_2$[11] and $Li_{1.2}Fe_{0.4}Ti_{0.4}O_2$[11]). It is possible to identify the cation distribution in cubic rock-salt phase as random distribution of Li, Mn, and Fe ions on both 3a and 3b sites in layered rock-salt one. In general, QS value tends to increase with an increase in local structure variation and distortion around the intended Fe ions. According to these considerations, QS data analysis reveals that Fe^{3+} ions in $Li_{1.2}Fe_{0.4}Mn_{0.4}O_2$ exists on both 3a and 3b sites, while Fe^{4+} ions exists only on 3b site. This is consistent with neutron diffraction results, which clarified that only Fe ions exist at 3a site in Li layer [6], as well as X-ray diffraction analysis; relatively small Fe^{4+} ions can exist at 3b site rather than 3a site, because the nearest metal-oxide ion (M_{3b}-O) distance between 3b and 6c sites (1.9862(10) Å) is smaller than that (M_{3a}-O) between 3a and 6c sites (2.1064(12) Å) in sample F2.

Additionally, the specific surface area of sample F2 (14.4 m^2 g^{-1}) was similar to that of sample F1 (11.5 m^2 g^{-1}), indicating that the difference in particle size between them is negligible.

To clarify the origin of the difference in cation distribution, two precursors obtained by hydrothermal reaction in step 2, named as samples H1 and H2, were examined. The samples H1 and H2 were used for preparing samples F1 and F2 in step 3, respectively. XRD data showed that both samples were mixture of α-$NaFeO_2$ type oxide and spinel ferrite ($Fd\bar{3}m$, a = 8.31–8.33 Å, Fig. 6). It was seen that the estimated spinel ferrite content of sample H2 (4%) by Rietveld analysis was smaller than that of sample H1 (11%). The formed spinel ferrite ($Fd\bar{3}m$) could be assigned as $LiFe_5O_8$ (a = 8.333 Å) rather than $MnFe_2O_4$ (a = 8.499 Å) from observed lattice parameter. The XRD analysis was supported by magnetization measurement; the $LiFe_5O_8$ contents were 1.1% for sample H2 and 6.9% for sample H1, assuming that only $LiFe_5O_8$ (spontaneous magnetization, σ = 65 Gcm^3 g^{-1}) exists as a magnetic impurity phase in both the samples, and that it had the same magnetization as the bulk. The formation of $LiFe_5O_8$ in precursor suggests that Fe-rich co-precipitate coexists with the Fe-poor one, because $LiFe_5O_8$ can precipitate at same hydrothermal reaction condition from the mixture of $LiOH{\cdot}H_2O$ and $Fe(NO_3)_3$ solution [12].

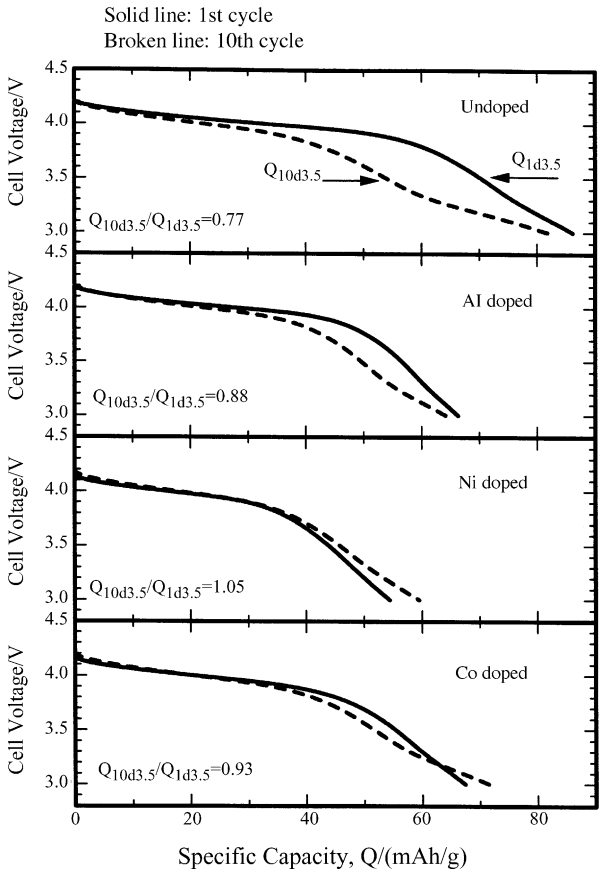

Fig. 8. Initial and 10th discharge curves after charging to 4.3 V for Li/sample cells when undoped and doped samples used as a positive electrode.

These results lead to a valuable conclusion; more homogeneous precursor could be obtained by adjusting the deposition temperature of Fe–Mn co-precipitate to −10 °C. Large difference in particle size was detected by TEM observation for both samples (Fig. 7); the average particle size of sample H2 (24 nm) was only half of that for sample H1 (48 nm), which was also calculated from their specific surface area. This means that sample H2 is expected to be more reactive with lithium sources than sample H1, and is a suitable precursor for obtaining the final product with high cation ordering at relatively low-temperature firing.

3.2. Effect of dopants on electrochemical properties

For all doped samples, the deposition temperature, the hydrothermal and firing conditions were fixed to −10 °C, 220 °C for 8 h and 650 °C for 20 h. No other impurity phase could be detected by XRD analysis for all of them. Elemental analysis showed that dopant content to total metal one except for Li was 2.6 mol% for Al, 4.9 mol% for Ni and Co. The cation doping was attained, however, a small loss of Al was observed. Cation distribution was not drastically changed after doping; $(Li_{0.9533}M_{0.0467(13)})_{3a}[M_{0.683(3)}Li_{0.317}]_{3b}O_2$ (M = Al, Fe and/or Mn) for Al-doped sample, $(Li_{0.9629}M_{0.0371(13)})_{3a}$

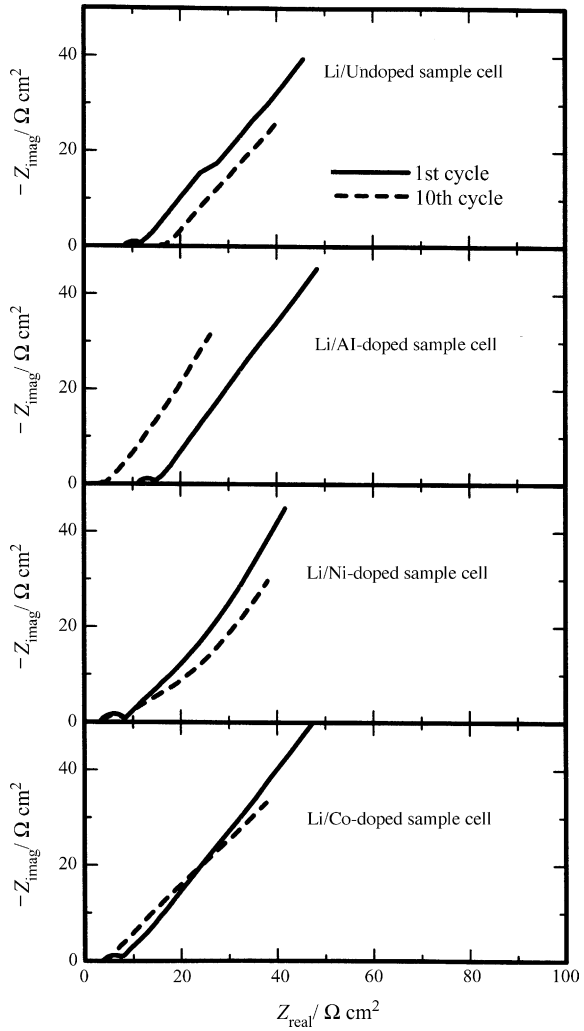

Fig. 9. Nyquist plots of Li/sample cells at 1st and 10th cycle at discharged state 3.0 V.

$[M_{0.660(3)}Li_{0.340}]_{3b}O_2$ (M = Ni, Fe and/or Mn) for Ni-doped one and $(Li_{0.9567}M_{0.0433(13)})_{3a}[M_{0.669(3)}Li_{0.331}]_{3b}O_2$ (M = Co, Fe and/or Mn) for Co-doped one.

Both the initial and 10th discharge capacities were reduced after doping (Fig. 8). However, degradation of the discharge capacity above 3.5 V from 1st to 10th cycles was significantly suppressed in the doped samples, the capacity retention above 3.5 V from 1st to 10th cycles ($Q_{10d3.5}/Q_{1d3.5}$) was improved from 0.77 for undoped sample (sample F2) to 0.88 for Al-doped one, 1.05 for Ni-doped one and 0.93 for Co-doped one.

AC impedance technique was used for considering about the difference in electrochemical performance between these cells (Fig. 9). The cell impedance was raised with an increase in the cycling from 1st to 10th cycle for Li/undoped sample cell on discharge states. In contrast, cell impedance was reduced for Li-/Al-doped sample cell and remained almost unchanged for Li-/Ni- and Co-doped sample ones. These results reveal that the cycle deterioration of charge and discharge capacities for Li-/undoped sample cell (Fig. 2) may be correlated with the increase in cell impedance, and the suppression of capacity degradation may be accomplished by other metal doping, which inhibits the raise of cell impedance.

There have been some experimental reports on the structural variation in Li_2MnO_3-based compounds during the electrochemical redox cycling. The oxygen loss during the charge process has been reported for NiO–Li_2MnO_3 solid solution [13] and the 3b–6c Cr disordering has been observed for $LiCrO_2$–Li_2MnO_3 solid solution [14]. In addition, we observed oxygen loss and Fe ion disordering from 3b to 6c sites in $Li_{1.2}Fe_{0.4}Ti_{0.4}O_2$ [11] and $LiCo_{0.8}Fe_{0.2}O_2$ [10] during the electrochemical tests, respectively. To understand the origin for discrepancy in the cell impedance with cycle, further studies on structural and compositional changes in positive electrode are required and carried out in near future.

4. Conclusions

The electrochemical performance of $Li_{1.2}Fe_{0.4}Mn_{0.4}O_2$ was improved by controlling the preparation temperature of Fe–Mn co-precipitate below RT. The improvement was attained mainly by lowering the 3d metal ion content in Li layer. The more cation ordered sample could be obtained from homogeneous and reactive precursor with relatively low spinel ferrite content.

The degradation of discharge capacity with cycle could be suppressed by Al, Ni and Co doping. These dopants can act as an inhibitor for increase in cell impedance with cycle number. This means that Fe-substituted Li_2MnO_3 will be considered for practical use by optimizing its preparation condition and chemical composition.

Acknowledgements

We express our gratitude for financial support from The New Energy and Industrial Technology Development Organization (NEDO) and Ministry of Economy, Trade and Industry (METI), and for valuable advices from Dr. Tatsuya Nakamura of Himeji Institute of Technology. We appreciate Mr. Yasutaka Ohno of Central Research Institute of Electric Power Industry for AC impedance measurement.

References

[1] R. Alcántara, J.C. Jumas, P. Lavela, J. Olivier-Fourcade, C. Pérez-Vicente, J.L. Tirado, J. Power Sources 81–82 (1999) 547–553.
[2] J.N. Reimers, E. Rossen, C.D. Jones, J.R. Dahn, Solid State Ionics 61 (1993) 335–344.
[3] H. Kobayashi, H. Shigemura, M. Tabuchi, H. Sakaebe, K. Ado, H. Kageyama, A. Hirano, R. Kanno, M. Wakita, S. Morimoto, S. Nasu, J. Electrochem. Soc. 147 (2000) 960–969.
[4] C. Delmas, M. Ménétrier, L. Croguennec, I. Saadoune, A. Rougier, C. Pouillerie, G. Prado, M. Grüne, L. Fournès, Electrochim. Acta 45 (1999) 243–253.

[5] M. Tabuchi, H. Shigemura, K. Ado, H. Kobayashi, H. Sakaebe, H. Kageyama, R. Kanno, J. Power Sources 97–98 (2001) 415–419.
[6] M. Tabuchi, A. Nakashima, H. Shigemura, K. Ado, H. Kobayashi, H. Sakaebe, H. Kageyama, M. Kohzaki, A. Hirano, R. Kanno, J. Electrochem. Soc. 149 (2002) A509–A524.
[7] S.H. Kang, J. Kim, M.E. Stoll, D. Abraham, Y.K. Sun, K. Amine, J. Power Sources 112 (2002) 41–48.
[8] F. Izumi, T. Ikeda, Mater. Sci. Forum 321–324 (2000) 198–203.
[9] M. Tabuchi, K. Ado, H. Kobayashi, I. Matsubara, H. Kageyama, M. Wakita, S. Tsutsui, S. Nasu, Y. Takeda, C. Masquelier, A. Hirano, R. Kanno, J. Solid State Chem. 141 (1998) 554–561.
[10] V.L. McLaren, A.R. West, M. Tabuchi, A. Nakashima, H. Takahara, H. Kobayashi, H. Sakaebe, H. Kageyama, A. Hirano, Y. Takeda, J. Electrochem. Soc. 151 (5) (2004) A672–A681.
[11] M. Tabuchi, A. Nakashima, H. Shigemura, K. Ado, H. Kobayashi, H. Sakaebe, K. Tatsumi, H. Kageyama, T. Nakamura, R. Kanno, J. Mater. Chem. 13 (2003) 1747–1757.
[12] M. Tabuchi, K. Ado, H. Sakaebe, C. Masquelier, H. Kageyama, O. Nakamura, Solid State Ionics 79 (1995) 220–226.
[13] Z. Lu, J.R. Dahn, J. Electrochem. Soc. 149 (7) (2002) A815–A822.
[14] Z. Lu, J.R. Dahn, J. Electrochem. Soc. 150 (8) (2003) 1044–1051.